Available online at www.sciencedirect.com
SCIENCE DIRECT
Polymer 46 (2005) 8846–8858
polymer
www.elsevier.com/locate/polymer

Structural deformation behavior of isotactic polypropylene with different molecular characteristics during hot drawing process

Takashi Sakurai[a,*], Yoshinobu Nozue[a], Tatsuya Kasahara[a], Kohji Mizunuma[a], Noboru Yamaguchi[a], Kohji Tashiro[b], Yoshiyuki Amemiya[c]

[a]*Petrochemicals Research Laboratory, Sumitomo Chemical Co., Ltd, 2-1 Kitasode, Sodegaura City, Chiba 299-0295, Japan*
[b]*Graduate School of Engineering, Toyota Technological Institute, Nagoya City, Aichi 468-8511, Japan*
[c]*Graduate School of Frontier Sciences, The University of Tokyo, Kashiwanoha, Kashiwa City, Chiba 113-8656, Japan*

Received 15 October 2004; received in revised form 20 January 2005; accepted 24 January 2005
Available online 12 July 2005

Abstract

Structural evolution in hot drawing process of isotactic polypropylene (iPP) films with different molecular weight distribution (MWD) and isotacticity (IT) was investigated by in situ time-resolved measurements of synchrotron-sourced wide-angle X-ray diffraction (WAXD) and small-angle X-ray scattering (SAXS). Any significant difference was not recognized among different molecular characteristics as for the changes in the WAXD patterns, indicating that the deformation behavior viewed at the crystal lattice scale was almost the same among these samples. On the other hand, the deformation behavior of lamellar stacking structure was found to be significantly dependent on the molecular characteristics of the sample used. For iPP sample with narrower MWD and higher IT, only the lamellar stacking structure with *c*-axis crystallites oriented along the drawing direction was detected at the deformation stage after necking, but the oriented fibrillar structure was observed in addition to the lamellar stacking structure for the iPP sample with broader MWD and IT distribution. The structural deformation models were presented for both the samples with different molecular characteristics, and these models were reasonably related with the difference in the stress–strain curve.

Keywords: Isotactic polypropylene; Hot drawing; Synchrotron

1. Introduction

Isotactic polypropylene (iPP) is extensively used in industry to manufacture bottles, films, and fibers, etc. The heat and draw deformation behavior of iPP is of significant practical importance in terms of both its product performances and manufacturing processes. The mechanical properties and morphology of the product are strongly affected not only by its molecular characteristics such as the molecular weight (MW), molecular weight distribution (MWD) and isotacticity (IT) [1–4] but also by its processing conditions such as the drawing temperature, the drawing ratio, the strain rate and the cooling rate after drawing [5–7]. Therefore, understanding the structural deformation behavior during processing is essential for the quantitative predictions of improved product performances and the drawing tension.

Structural deformation behavior over a wide range of strain and temperature has been actively studied from scientific and industrial aspects for many years, i.e. spherulite deformation [8–12], necking behavior [13,14] and ultradrawability [15]. It is widely recognized that, when the semicrystalline polymers are drawn, the lamellar crystallites in the spherulites are more or less destroyed (decreased in size and/or reduced in perfection) by the shear forces followed by the reformation of different morphology depending on the temperature of drawing. According to the microfibril model proposed by Peterlin [16] for the structural deformation process, the thus drawn films or fibers consist of aligned small lamellar blocks, which are connected with each other through non-crystalline tie molecules or crystalline bridges. But there have been several reports that do not support such a transition scheme of crystal lamellae into microfibrils and a longitudinal sliding motion of these microfibrils [15,17,18]. Some papers

* Corresponding author.

0032-3861/$ - see front matter © 2005 Elsevier Ltd. All rights reserved.
doi:10.1016/j.polymer.2005.01.106

describe the melt of crystalline lamellae under tension followed by the recrystallization into oriented fibrillar structure. At present we have no established general model for the drawing behavior of the crystalline polymer samples.

In order to trace the structural evolution in hot drawing process, we need to perform time-resolved measurements of various experimental data. For example, wide-angle X-ray diffraction (WAXD) is useful for the investigation of structural change in the crystal lattice. Small-angle X-ray scattering (SAXS) is a useful tool for the study of stacked lamellar structure. In order to collect the WAXD and SAXS data in the drawing process in a short time interval, synchrotron radiation is one of the most powerful tools [19–23]. A combination of this synchrotron radiation and the high-speed and high-sensitivity CCD detector enables us to collect the WAXD and SAXS data in a second with a high signal-to-noise ratio [24]. Hsiao and co-workers [19,20] studied the structural changes of iPP under uniaxial tensile force and discussed the deformation-induced crystalline transformation. However, they treated the structural deformation in narrow range of strain using a fiber of iPP polymerized by conventional Zieglar–Natta type catalyst system. In the actual manufacturing process of iPP film, the material is stretched as much as possible at a high temperature to produce the film with high tensile strength and good transparency. Hence, it is significantly important to investigate the structural deformation behavior of the films during hot drawing process in much wider strain range from the unoriented to largely deformed state where it is broken off. Besides, as pointed out above, the morphology and mechanical properties of the drawn films should be affected strongly by molecular characteristics such as MW, MWD and IT. It may be reasonably expected that the samples with different molecular characteristics should show different structural deformation behaviors in the hot drawing process even under the same conditions [25]. In other words the molecular characteristics are key factors necessary for improving the product performances and drawing tension. Unfortunately, there had been, however, no report describing an effect of molecular characteristics on the deformation behavior of iPP samples from the microscopic point of view.

The present paper is the first trial to clarify the relation among the molecular characteristics, the mechanical deformation behavior and the structural change of crystalline lamellae during the hot drawing process for iPP films with various types of molecular characteristics. We will describe the mechanical deformation behavior and its relation with the structural change in the hot drawing process, which were revealed for the various types of iPP samples on the basis of the measurement of the stress–strain curves and time-resolved measurement of WAXD and SAXS patterns with synchrotron radiation. The effect of MWD and IT on the mechanical deformation behavior will be discussed in detail.

2. Experiment

2.1. Materials

The characteristics of iPP samples are listed in Table 1; the iPP polymerized by conventional Ziegler–Natta catalyst system (zPP), the fraction of zPP insoluble in boiling *n*-heptane (BHIS), the fraction of zPP insoluble in boiling octane (BOIS), and the iPP polymerized by metallocene catalyst system (mPP). The polymerization of mPP was made following the procedures reported already [26]. The BHIS and BOIS were prepared by solvent extraction of zPP with boiling *n*-heptane and *n*-octane in a Soxhlet extractor, respectively. Each iPP sample except BHIS and BOIS was completely dissolved in boiling *p*-xylene, and then the solution was cooled gradually to 20 °C. The precipitated fraction was separated from the solution by filtration. The fraction soluble in *p*-xylene at 20 °C (CXS) was recovered from the filtrate by evaporation of the solvent. The isotactic pentad fraction [mmmm] was estimated by ^{13}C NMR with a Bruker AVANCE-600 spectrometer at a ^{13}C resonance frequency of 150 MHz at 135 °C. The *ortho*-dichlorobenzene solutions at 10 wt% concentration were used for ^{13}C NMR measurements. The analysis of [mmmm] was made by following the procedures reported elsewhere [27–30]. The MW and MWD of iPP samples were determined at 145 °C with a Millipore Waters 150-CV gel permeation chromatography apparatus. Three Shodex AT-806MS columns were applied and the solvent used was *ortho*-dichlorobenzene. Intrinsic viscosity [η] of iPP samples was measured by Ubbelohde viscometer for 1,2,3,4-tetrahydronaphthalene solutions at the concentration of 0.1 wt% at 135 °C.

A schematic illustration of the distribution of MW and IT of four iPP samples is shown in Fig. 1. More detailed description was reported in the previous paper [31]. The zPP has wide distribution of MW and IT around the averaged values. The BHIS and BOIS samples have narrower MWD, higher IT and narrower distribution of IT compared with those of zPP. The mPP sample has also higher IT and narrower distribution of MW and IT than zPP, but it does not contain the fractions with lower and ultra-higher MW components.

Crystallization and melting temperatures (T_c and T_m) were determined by means of a Perkin–Elmer DSC7 instrument. The calibration of temperature was made by checking the melting temperature of indium (156.6 °C). The iPP samples of ca. 10 mg were first heated to 220 °C, held there for 5 min, then cooled to 50 °C at a rate of 5 °C min^{-1} and reheated to 180 °C at the same rate in a nitrogen atmosphere. In both crystallization and melting experiments the peak temperatures were read out for T_c and T_m values. The crystallinity of the samples was evaluated by the density method on the basis of a two-phase model by assuming the crystalline and amorphous densities of 0.936 and 0.853 g cm^{-3}, respectively [32]. Density measurements

Table 1
Characteristics of iPP samples

Sample	M_w[a]	M_w/M_n[a]	CXS fraction[b] (wt%)	[mmmm][c]	$[\eta]$[d]	T_m[e] (°C)	T_c[e] (°C)	Density (g/cm^3)	Crystallinity (wt%)
zPP	435,600	5.1	4.0	0.91	2.10	160.9	117.6	0.901	59
BHIS	417,100	3.5	–	0.95	2.12	161.9	119.6	0.904	63
BOIS	726,000	2.3	–	>0.99	2.76	164.2	122.1	0.909	68
mPP	364,300	1.9	0.1	>0.99	2.20	160.1	118.8	0.905	64

[a] Determined by GPC (Waters, 145 °C).
[b] Fraction soluble in *p*-xylene at 20 °C.
[c] Isotactic pentad fraction determined by ^{13}C NMR (Bruker, 150 MHz at 135 °C).
[d] Intrinsic viscosity determined by Ubbelohde viscometer.
[e] Crystallization and melting temperatures determined by DSC.

were carried out at 30 °C with a density gradient column consisting of the mixtures of propan-2-ol and diethylene glycol to give a density range from 0.860 to 0.925 g cm^{-3}.

2.2. Drawing

The iPP specimens were cut out into the shape shown in Fig. 2 from the sheets prepared by pressing at 230 °C, held there for 5 min, then cooled to 30 °C in water bath. Semicircular notches were cut at the center of the specimen so that the necking phenomenon started to occur at the center of the specimen and then the necked area propagated along the edge sides. The specimen was set in a tensile tester installed in the path of synchrotron X-ray beam (Fig. 2). It was kept at 120 °C for 5 min and was drawn uniaxially at a strain rate of 20 mm/min at 120 °C. The stress was estimated from the tensile force divided by the initial cross-sectional area. The draw ratio (DR) was determined from the distance between marks printed on the specimen. The DR was estimated from the draw strain in the stress/strain curve as DR = %strain/100 + 1.

2.3. Time-resolved measurements

Synchrotron WAXD and SAXS measurements were carried out at BL-15A of Photon Factory, High Energy Accelerator Research Organization, Japan. The wavelength used was 1.504 Å. For tracing the structural change in the specimen during hot drawing process, time-resolved two-dimensional (2D) WAXD and SAXS patterns were measured at the center of the stretching film (beam size 1.0 × 1.0 mm^2) with a 1 s time slice by using a CCD X-ray detector [33,34]. The sample-to-detector distances for the WAXD and SAXS measurements were 100 and 2250 mm, respectively. From the thus measured 2D WAXD and SAXS patterns, the WAXD and SAXS intensity profiles along and perpendicular to the drawing direction were evaluated. Long period along the drawing axis was also evaluated from the 2D SAXS data.

3. Results and discussion

3.1. Mechanical properties

Fig. 3 shows the stress–strain curves of zPP and mPP

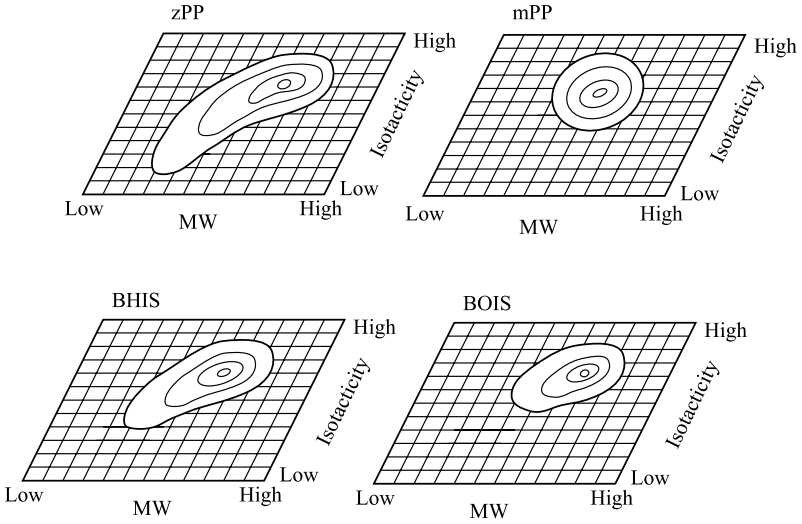

Fig. 1. The schematic illustration of distribution of molecular weight and isotacticity estimated for the various types of iPP samples.

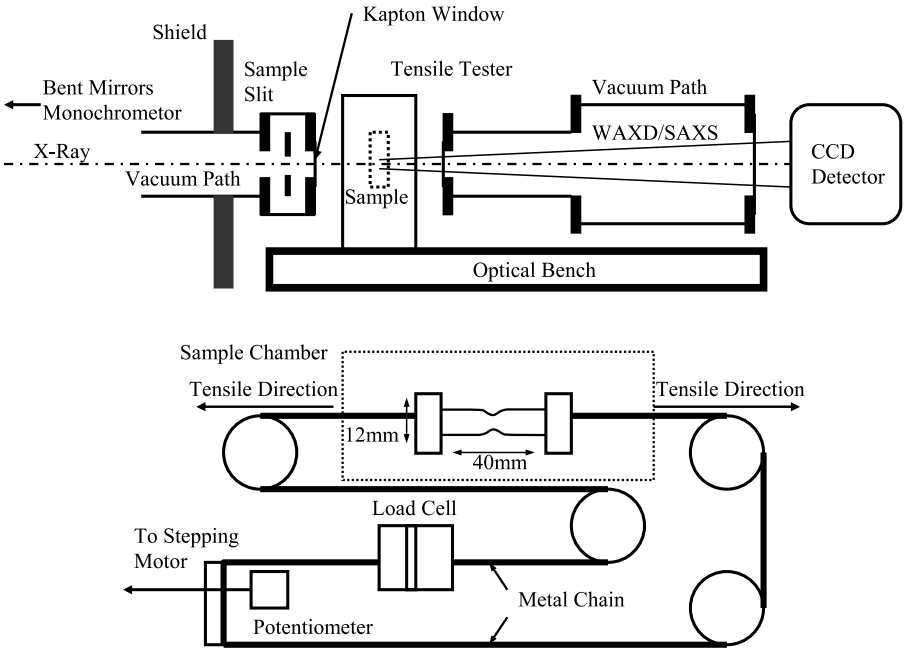

Fig. 2. The schematic illustration of experimental assembly and tensile machine.

samples measured at a strain rate of 20 mm/min at 120 °C. The samples gave a well-defined yield point followed by a steep drop in stress when the necking phenomenon occurred. Then the gradual increase of tensile stress was observed in the further drawing region. The characteristic features of the stress–strain curves obtained for the other types of iPP samples were similar with those of zPP and mPP samples. The whitely opaque parts were slightly recognized for the BOIS sample in the hot drawing process. Neither fracture nor opaqueness was observed for the other iPP samples, suggesting that the formation of craze and/or crack did not occur in the hot drawing process. In Table 2 are listed the yielding stress and the rate of stress increment in the draw region beyond the necking. The mPP and BOIS samples showed higher yielding stress and the rate of stress increment than zPP and BHIS.

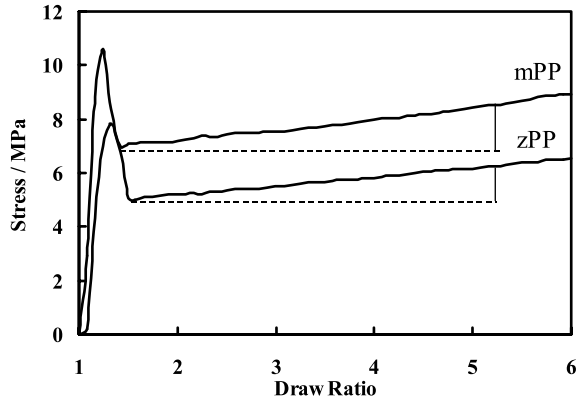

Fig. 3. The stress–strain curves of mPP and zPP samples. Dashed line is a guide helpful to speculate the rate of stress increment in the draw region beyond necking. The strain rate was 20 mm/min and the drawing temperature was 120 °C.

Fig. 4 shows the crystallinity dependence of yielding stress evaluated for the iPP samples that have nearly the same molecular characteristics as those used in the experiments except for MW. It was confirmed that the yielding stress increased with an increase in the degree of crystallinity. This relation is almost common to all the types of iPP samples used in the experiments. In Fig. 5 is plotted the crystallinity and intrinsic viscosity dependence of the rate of stress increment in the draw region beyond the necking. Fig. 5(a) shows that the rate of stress increment does not seem to have correlation with the degree of crystallinity. On the other hand, the rate of the stress increment seems to decrease with lowering intrinsic viscosity (with the lowering MW), as shown in Fig. 5(b). Both zPP and mPP samples show almost linear relation between the stress increment rate and the intrinsic viscosity. But the value of the rate of the stress increment itself is significantly different between these two samples. This difference is considered to come from the difference in morphology as will be discussed in a later section.

Table 2
Yielding stress and rate of stress increment

Sample	Yielding stress (MPa)	Rate of stress increment (kPa/mm)
zPP	7.7	58
BHIS	10.3	72
BOIS	11.7	78
mPP	10.5	80

Estimated from stress–strain curve (Fig. 3).

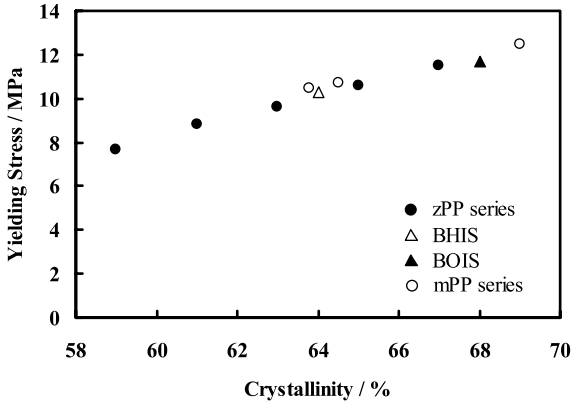

Fig. 4. The relationship between yielding stress and crystallinity. (●), iPP polymerized by Ziegler–Natta catalyst system; (○), iPP polymerized by metallocene catalyst system; (△), BHIS; (▲), BOIS.

3.2. WAXD measurements

2D WAXD patterns of zPP and mPP observed in hot drawing process are shown in Fig. 6. The 2D WAXD pattern before drawing (DR = 1.0) exhibited the Debye–Scherrer rings. These rings were changed into the arcs at the onset of necking in the stress–strain curve, and the azimuthal spread of the reflections became narrower with increasing DR, indicating an enhancement of *c*-axis crystallites oriented along the drawing direction. The three intense peaks on the equatorial direction, which are characteristic of the α-crystal form, are indexed as 110, 040 and 130 reflections, respectively [35].

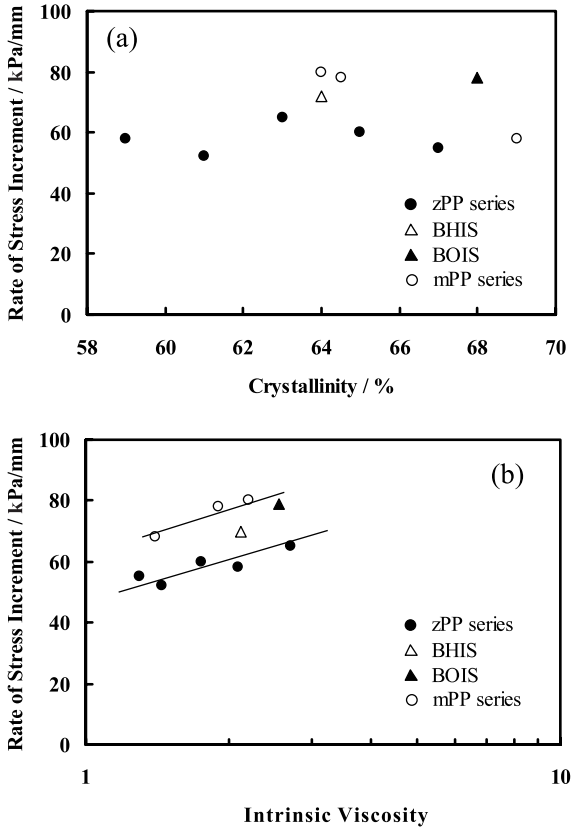

Fig. 5. The relationship between stress increment and (a) crystallinity and (b) intrinsic viscosity. (●), iPP polymerized by Ziegler–Natta catalyst system; (○), iPP polymerized by metallocene catalyst system; (△), BHIS; (▲), BOIS.

Fig. 7 shows the DR dependence of intensity profiles of zPP and mPP extracted along the equatorial direction of the WAXD patterns shown in Fig. 6. The positions of the three intense peaks are almost constant during hot drawing process, but their widths become broader with increasing DR. The diffraction peaks of 110, 040 and 130 remain only on the equatorial lines in the DR region beyond necking, indicating that the *c*-axis crystallites orient along the drawing direction. The DR dependence of the full width at half maximum (FWHM) of the diffraction profile is evaluated for the 110, 040 and 130 reflections as shown in Fig. 8. The increment of the FWHM means that the crystallites become smaller in size and/or disordered remarkably in the draw region before necking. After necking, FWHM increased gradually. In Fig. 8 any significant difference was not recognized among the four types of iPP samples as for the changes in 2D pattern and 1D profile of the WAXD.

3.3. SAXS measurements

Fig. 9 shows the time dependence of the 2D SAXS patterns of zPP and mPP in hot drawing process. The 2D SAXS pattern of zPP before drawing showed a broad ring. It transformed to elliptical pattern around yielding point (DR = 1.2). In the draw region beyond the yielding point, the 2D SAXS pattern showed a two-bar pattern with the scattering maximum on the meridional direction (DR ≥ 1.3) and the streak-like pattern along the equatorial direction (DR ≥ 1.4). The two-bar pattern gradually shifted toward the lower scattering angle side, and the intensity became gradually weaker with increasing DR. In the case of mPP, the two-bar pattern was also obtained in the necking region but the scattering intensity decreased more rapidly with increasing DR than the case of zPP. The 2D SAXS patterns of four types of iPP at DR = 6 are compared in Fig. 10. Different from the cases of zPP and BHIS, mPP and BOIS did not have an appreciable streak on the equatorial direction, where the streak on the equatorial direction observed for BOIS was attributed to the scattering due to crazing.

Fig. 11 shows the DR dependence of SAXS intensity profiles obtained from Fig. 9 along the equatorial and meridional directions. As for the SAXS intensity profile along the meridional direction shown in Fig. 11(a) and (c), there are at least two significant experimental tendencies. One is about the peak position and intensity due to the long period. As the drawing ratio increased from DR = 1.0 to 1.2, the peak position shifted to lower scattering angle, being accompanied with the decrease in peak intensity. In the draw region beyond necking (DR = 1.3–1.5) the peak

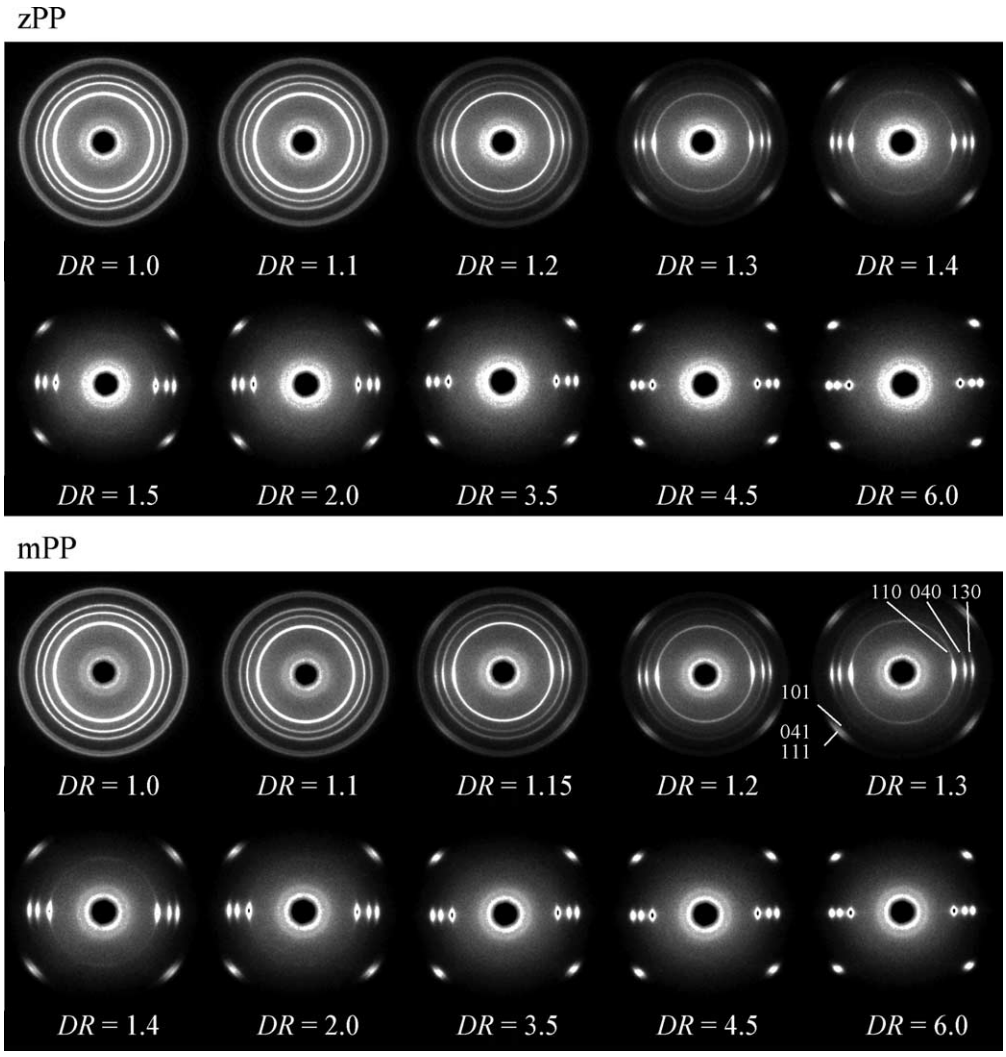

Fig. 6. The 2D WAXD patterns of zPP and mPP observed in the hot drawing process.

shifted back to higher angle, though only slightly, and then it shifted again toward the lower scattering angle (DR > 1.5). The peak intensity became gradually weaker with increasing DR. The other is about the FWHM and intensity of SAXS intensity profile during necking. The FWHM becomes narrower and the peak intensity increases during necking. The quantitative analysis of the long period, FWHM and the peak intensity changes is described in the following.

On the other hand, as to the SAXS intensity profile in the equatorial direction, the intensity due to long period became weaker during necking. After DR > 1.5, a streak, which had a broad maximum, started to appear in the case of zPP, but not in the case of mPP as shown in Fig. 11(b) and (d). This suggests an existence of periodical array of some crystalline entities in the zPP sample along the equatorial direction. There may be another possibility that such a maximum is related with the shape of a crystallite or aggregated crystallites, but the detailed discussion is not made here. This peak on the streak was not detected in the DR region beyond DR = 2.0. To the contrary, any clear peak was not detected in the SAXS profile of mPP on the equator.

Fig. 12 shows the change in peak intensity of zPP and mPP as a function of DR. The peak intensity decreased in necking regions, increased drastically after necking and again decreased gradually with further increasing DR. The mPP showed higher rate of the decrease in the peak intensity before and during necking. The DR dependence of FWHM of SAXS profile on the meridian is shown in Fig. 13, where the FWHM was estimated as a twice of HWHM of the higher scattering angle of the profile. The FWHM decreased drastically in the draw region before necking, kept the constant value for a while after necking and increased slightly with further increasing DR. The decrement of the FWHM means that the distribution of the long period of stacked lamellar structure becomes narrower. Fig. 14 shows the change of long period as a function of DR. As shown in Fig. 14(a) the long period before drawing is found to be related with the MW of the iPP samples: the long period is longer for the sample with higher MW. At the first stage of

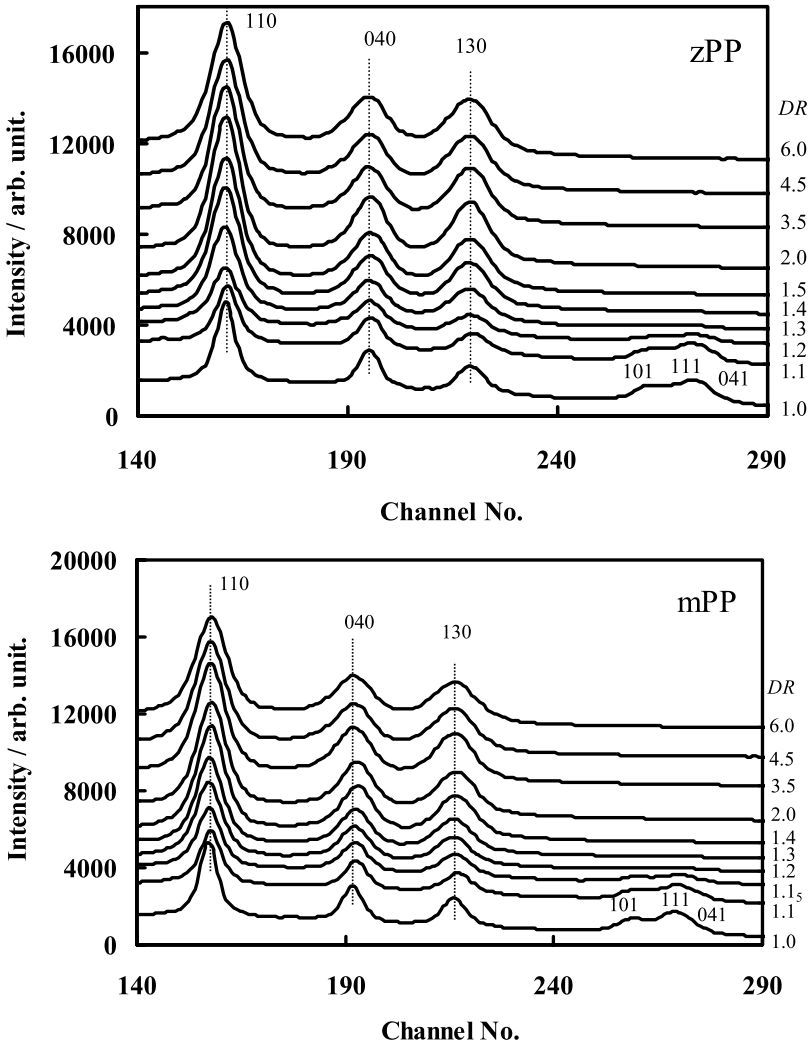

Fig. 7. The DR dependence of WAXD profile of zPP and mPP samples obtained along the equator of the WAXD pattern given in Fig. 6.

drawing, the long period increased steeply. After necking the long period decreased slightly (DR = 1.3–1.5) and then it increased again nearby linearly with increasing DR in the draw region beyond necking (DR > 1.5). In order to compare more clearly the long period change in the draw region beyond necking, the long period at each DR was normalized by dividing it by the long period L_o obtained at the point just beyond necking (DR = 1.3). Fig. 14(b) shows the thus normalized long period plotted against the DR. The slope of the straight line or the increasing rate of the long period was in the order of zPP < BHIS < BOIS < mPP. That is to say, the iPP sample with narrower MWD and higher IT shows the higher rate of long period change when stretched in the region after necking.

3.4. Structural interpretation of WAXD and SAXS patterns

Synchrotron WAXD and SAXS data tell us deformation of lamellar stacking structure and disorder in crystallites. In the necking region the crystallites are considered to become disordered remarkably as known from the increasing FWHM of the WAXD data. Besides the tilting and sliding of chains in the lamellae should occur at the same time [23]. The complicated change of the long period and the decrease in the SAXS intensity are considered to reflect such a remarkable change in the lamellar arrangement and a structural change in the lamellar crystallites. As implied in the FWHM change of Fig. 13, the distribution of the long period of the stacked lamellae before drawing seems to become narrower through the necking. After necking (DR > 1.5), the crystallites are considered to reduce structural perfection and become disordered gradually as estimated from the FWHM of the WAXD data (Fig. 8). Slower change of the long period and the decrease in the SAXS intensity suggest that the lamellar structure aligned along the drawing direction is gradually fragmentized [20]. This tendency is more remarkable for mPP sample.

In addition to the commonly-observed two-bar pattern with the scattering maximum on the meridional direction, the 2D SAXS pattern of zPP shows the streak-like pattern on

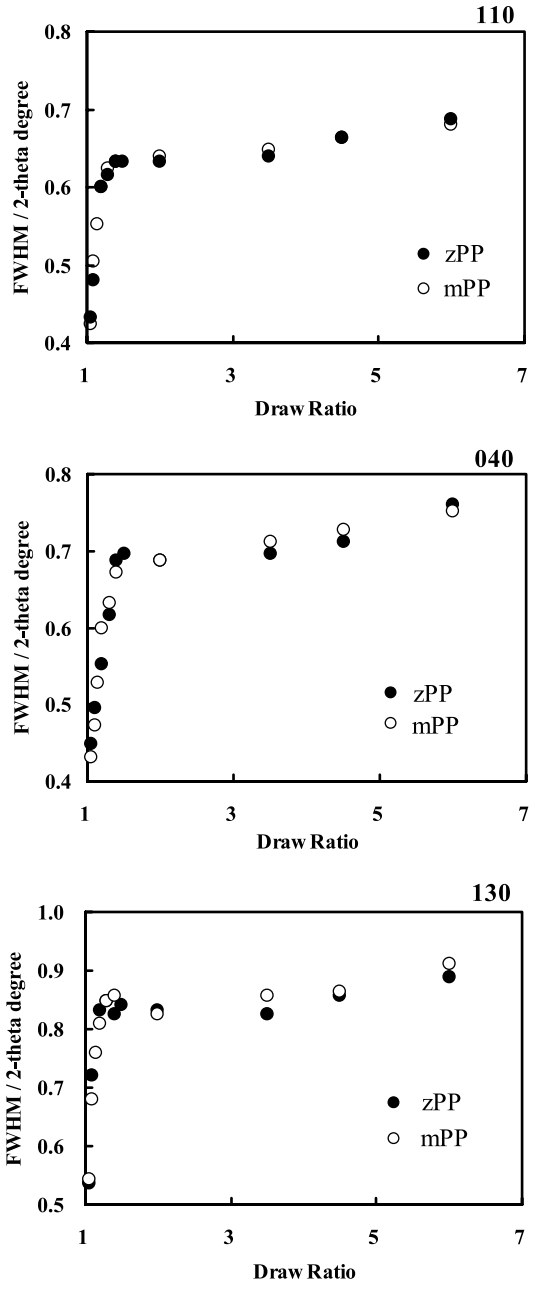

Fig. 8. The DR dependence of full width at half maximum intensity (FWHM) of the diffraction profile along the equator estimated for 110, 040 and 130 reflections, respectively.

the equatorial direction. This streak is clear for the zPP sample but is hard to observe for mPP sample. As shown in Fig. 10, the scattering intensity of the streak is weaker for the iPP samples (BOIS and mPP) with narrower MWD, higher IT and narrower distribution of IT (Fig. 1). As an origin of the streak, we may imagine an existence of a group of fibrils that lack axial register of crystalline regions. It is noted here in Fig. 9 that the streak observed in the region of DR = 1.4–2.0 is not perfectly directed in the equatorial direction but splits into two directions deviated slightly from it, probably reflecting a slight tilt of the fibrillar structures. Another point to note is that the streak has a maximal intensity on the way along the streak direction as shown in Figs. 9 and 11(b) (DR = 1.4–2.0), suggesting that these fibrillar structures form some periodical array. As another possible origin of the intensity maximum along the streak direction we might consider an existence of the lamellae stacked along the direction perpendicular to the draw axis. But such a possibility may be low because no WAXD spots corresponding to such perpendicularly-oriented lamellae were observed in Fig. 6. By drawing the sample further the streak is observed along the equatorial direction.

3.5. Relationship between structural deformation and mechanical properties

3.5.1. Stacked lamellar structure before drawing

As known from the preparation conditions described in the experimental section, the samples used here commonly consist of the α-crystal form crystallites in the spherulites. But, FWHM in SAXS intensity profile of zPP before drawing is wider than that of mPP as shown in Fig. 13, suggesting that the zPP has broader distribution of long period of the stacked lamellae than the mPP. As seen in Fig. 1, the zPP has broader MWD and broader distribution of IT and it is considered to contain molecular components of different characters. Therefore, we may say that the lamellar structure in the spherulites of zPP is highly heterogeneous. It is considered that some of the stacked lamellae may be broken into fibrillar structure that lacks axial register of crystalline regions as mentioned before, while the other lamellae are not deformed very much. Such a heterogeneous deformation of the lamellae gives both a two-bar pattern with the scattering maximum on the meridional direction and the streak-like pattern along the equatorial direction as seen in Fig. 9. On the other hand, the lamellar structure of mPP is considered to be relatively homogeneous because of the relatively narrow MWD and IT distribution. The stacked lamellae are oriented regularly along the drawing direction, giving relatively simple SAXS pattern compared with zPP case. That is to say, the fibrillar structure without any axial register of crystallites as detected for the zPP sample, is not observed for mPP after necking.

3.5.2. Deformation model during hot drawing process

A structural deformation model in hot drawing process is given schematically in Fig. 15. The marks a, b, c, etc. located near the stacked lamellar models are helpful for tracing the structural change in a series of pictures. The lamellae of mPP with narrower MWD, higher IT and narrower distribution of IT are deformed in more homogeneous manner. Before drawing (DR = 1.0) the stacked lamellae are oriented randomly in the spherulite as is indicated by the WAXD and SAXS patterns consisting of rings. By drawing this spherulite (DR = 1.2) the large lamellae are broken and the broken lamellae start to reorient

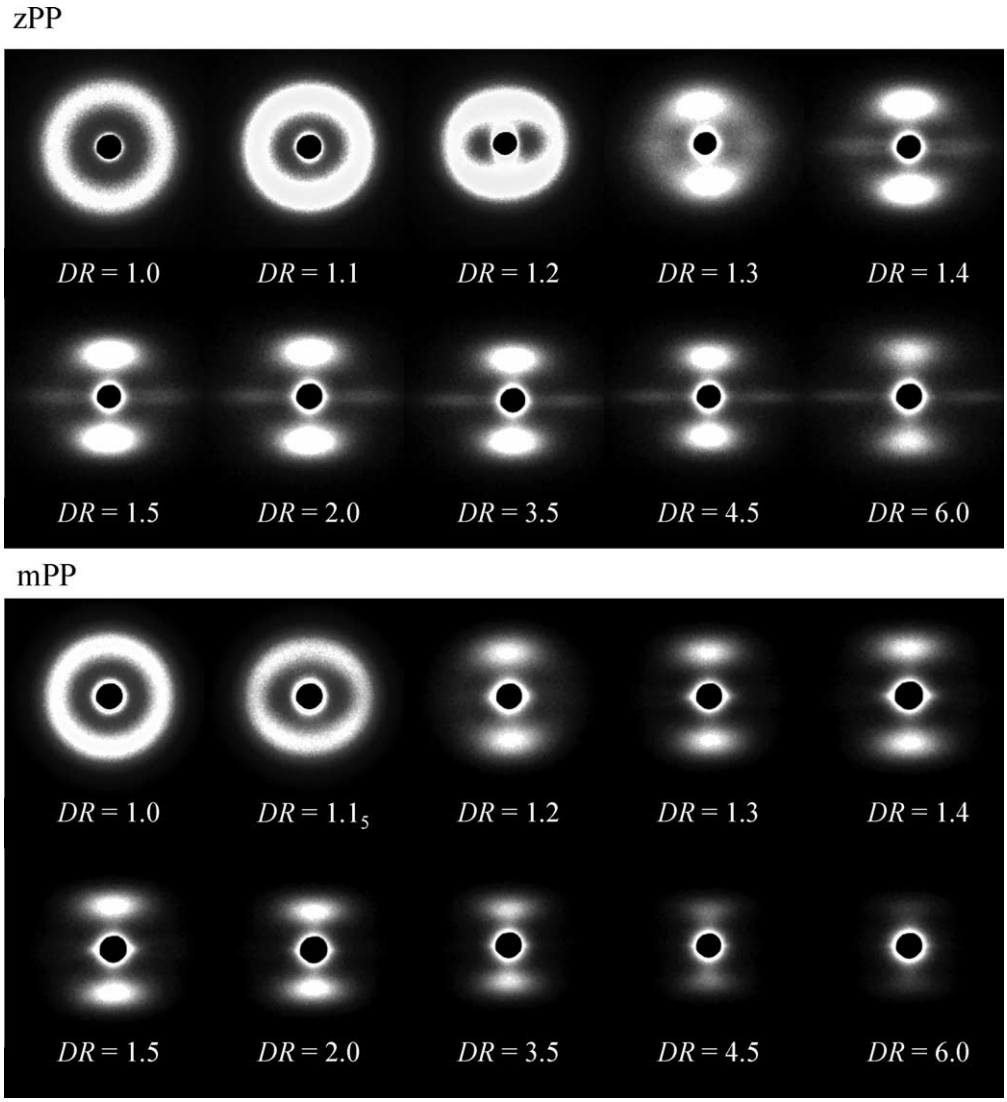

Fig. 9. The 2D SAXS patterns of zPP and mPP taken in the hot drawing process.

along the draw direction by tilting and sliding motions (a→a′). The WAXD pattern changes into the arcs and the SAXS gives an elliptical pattern. At DR = 2.0 the lamellar structures with *c*-axis crystallites oriented along the drawing direction are formed (a′→a″). The WAXD pattern shows the *c*-axis crystallites oriented along the drawing direction and SAXS pattern changes to the two-bar pattern. By drawing further (DR = 6.0), the fragmentation process proceeds in the lamellar structures formed along the drawing direction (a″→a‴). The WAXD gives *c*-axis crystallites highly oriented along the drawing direction and the SAXS intensity decreases with the shift toward the lower scattering angle side.

On the other hand, the zPP sample is speculated to contain the lamellae of various sizes because it has wide distribution of MW and IT (a, b, c). The deformation of lamellae in the necking region is more complicated than the case of the mPP sample. At DR = 1.2, the large lamellae in the spherulite are broken and start to reorient along the draw direction by tilting and sliding motions (a, b, c→a′, b′ c′). The WAXD pattern changes into the arcs and the SAXS pattern gives an elliptical pattern. At DR = 2.0, the lamellar structures with *c*-axis crystallites oriented along the drawing direction are formed (a′ and b′→a″ and b″). In some regions, the lamellae are deformed further to change into fibrillar structure and the stretched chains are gathered together to form the crystalline region that lacks axial register of crystalline regions (c′→c″). In this way, in the draw region after necking, the disordered fibrillar structure and the stacked lamellar structure are considered to coexist in the zPP sample. The WAXD pattern corresponds to the *c*-axis crystallites oriented along the drawing direction and the SAXS gives the two-bar pattern and the streak-like pattern. As the drawing ratio increases (DR = 6.0), the fibrillar structure seems to be stretched along the drawing direction furthermore (c″→c‴). The streak shifts to the equatorial direction. On the other hand the lamellae a″ and b″ are gradually fragmentized into smaller ones and the SAXS

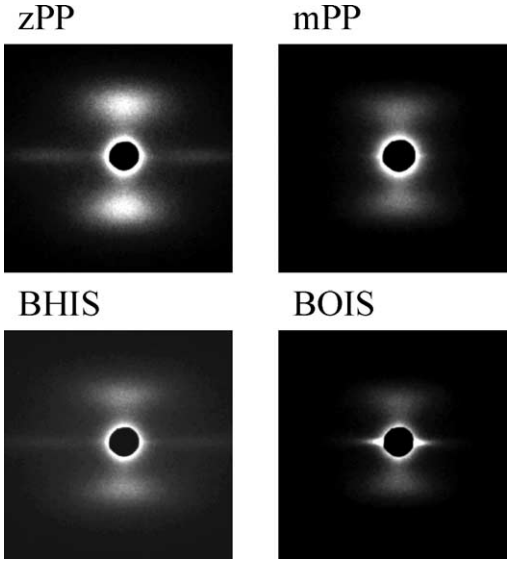

Fig. 10. Comparison of 2D SAXS patterns at DR = 6.0 between the various types of iPP samples.

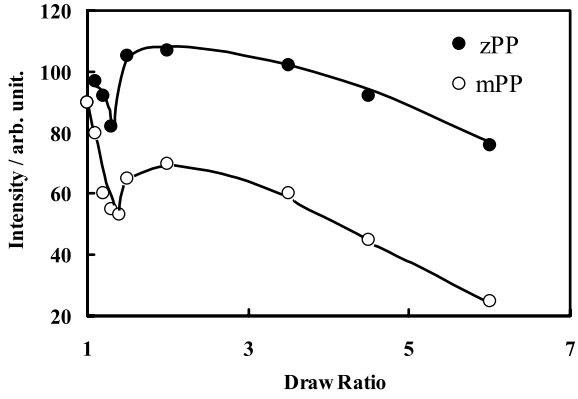

Fig. 12. The change of peak intensity on the meridian as a function of DR.

intensity decreases gradually ($a'' \rightarrow a'''$ and $b'' \rightarrow b'''$). This results in the apparently smaller change of long period in the drawing process. The WAXD gives the pattern of the *c*-axis crystallites highly oriented along the drawing direction. The lamellar structure of the thus oriented zPP sample is inhomogeneous, and it should give the inhomogeneous stress distribution in the sample when it is subjected to an external force.

3.5.3. Structure–property relationship

In this way the WAXD and SAXS data reveal a large difference in the deformation behavior between the zPP and mPP samples. The deformation is speculated to occur

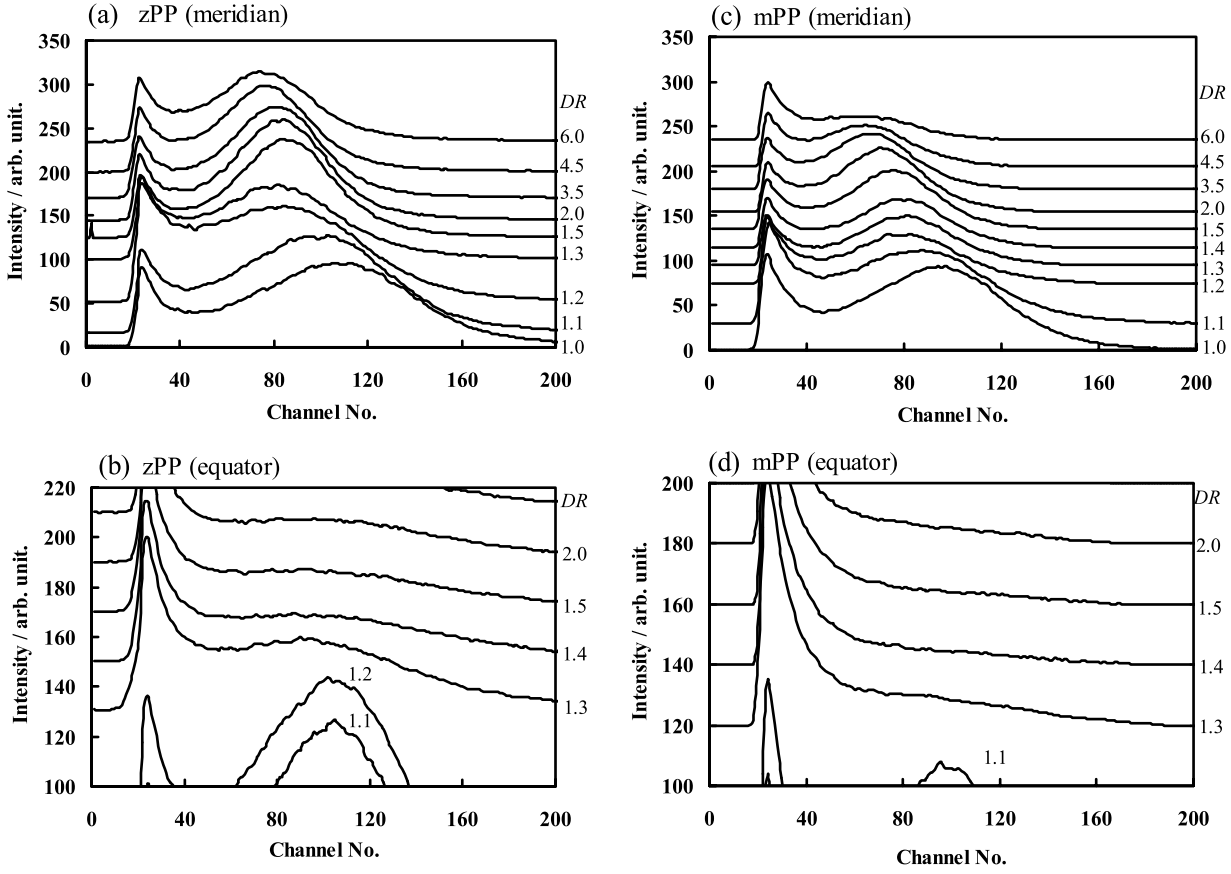

Fig. 11. The DR dependence of SAXS intensity profile obtained from SAXS pattern given in Fig. 9. (a) The SAXS intensity profile of zPP along the meridional direction. (b) The SAXS intensity profile of zPP along the equatorial direction. (c) The SAXS intensity profile of mPP along the meridional direction. (d) The SAXS intensity profile of mPP along the equatorial direction.

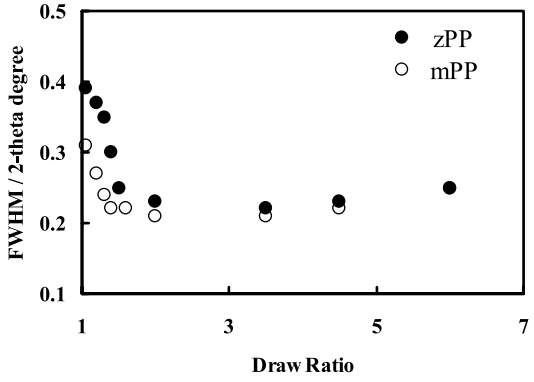

Fig. 13. The DR dependence of FWHM of SAXS intensity profile on the meridian.

cooperatively for the mPP sample. The necking region detected in the stress–strain curve is relatively narrow (Fig. 3) and the SAXS intensity profile change is comparatively simple. The higher stress increment in the drawing region may be interpreted also on the basis of such a homogenous deformation mechanism of mPP (Figs. 3 and 5 and Table 2). The cooperative and homogeneous deformation of the whole lamellae is considered to need relatively higher stress, resulting in the higher stress of the mPP sample compared with that of the zPP sample. On the other hand, the zPP sample containing wider distribution of MW and IT behaves in a heterogeneous manner. In the draw region after necking, the disordered fibrillar structure and the stacked lamellar structure are considered to coexist in the zPP sample. The former structure would give the lower tensile stress because of the lower chain entanglement and the easier slippage in the hot drawing process. This inhomogeneous stress distribution may be evaluated concretely by analyzing the infrared spectral change caused by an application of tensile force, as will be reported elsewhere.

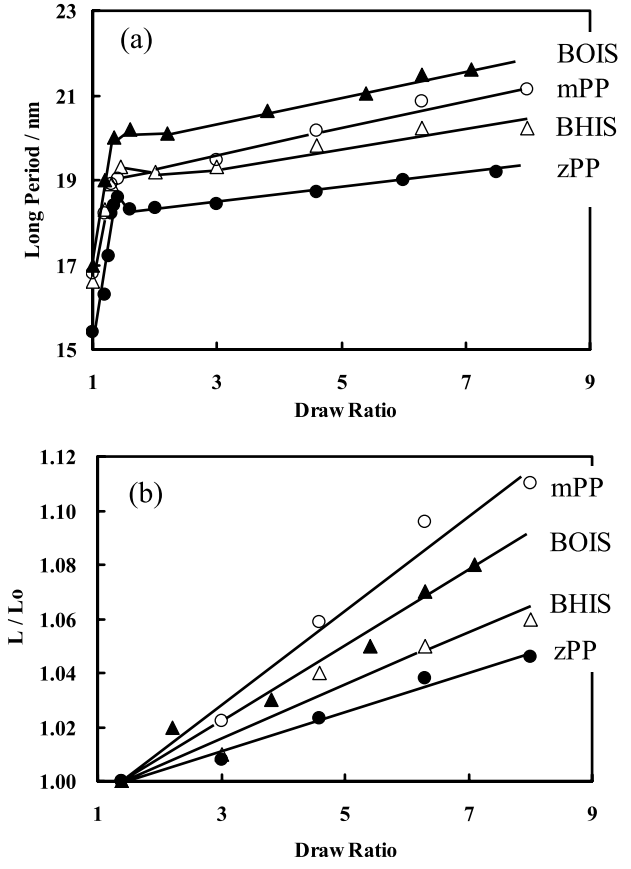

Fig. 14. (a) The changes of the long period as a function of DR. (b) The normalized long period plotted against the DR in the region after necking point.

The relationship between the lamellar deformation behavior and the molecular characteristics revealed for the mPP and zPP samples can be applied reasonably to the deformation processes observed for the other samples such as BOIS and BHIS. The BOIS sample has relatively narrower distribution of MW and IT and it shows the deformation behavior similar to that of mPP, while the BHIS sample has broader distribution of MW and IT and behaves similarly to the zPP sample. In fact, all the observations including the long period change in Fig. 14, the SAXS pattern at DR = 6.0, and so on are similar between zPP and BHIS and between mPP and BOIS. In other words, the iPP with narrower distribution of MW and higher IT shows more homogeneous structural change of lamellae in the hot drawing process.

4. Conclusions

In the present paper we have investigated the structural change and mechanical behavior during hot drawing process of iPP samples with various molecular characteristics on the basis of time-resolved synchrotron WAXD and SAXS measurements. We have found out for the first time that the difference in MW, MWD and IT gives quite large difference in the mechanical deformation behavior of iPP samples. The mPP sample with narrower MW and IT distributions exhibits more homogeneous lamellar stacking structure and the deformation of lamellae occurs cooperatively. The zPP sample prepared by Ziegler–Natta-type catalytic system and containing wider distribution of MW and IT behaves in a heterogeneous manner. The BOIS and BHIS samples behave in intermediate manner between these two samples.

In this way the iPP samples synthesized with different catalytic systems or different MW, MWD and IT distribution were found to behave in quite different manner when the samples were drawn at high temperature: they show different deformation behavior, different mechanical property, different morphology and different stress distribution. This finding is quite important in such a point that the mechanical property of iPP sample is affected sensitively not only by the external condition of drawing temperature, annealing temperature, etc. but also by the

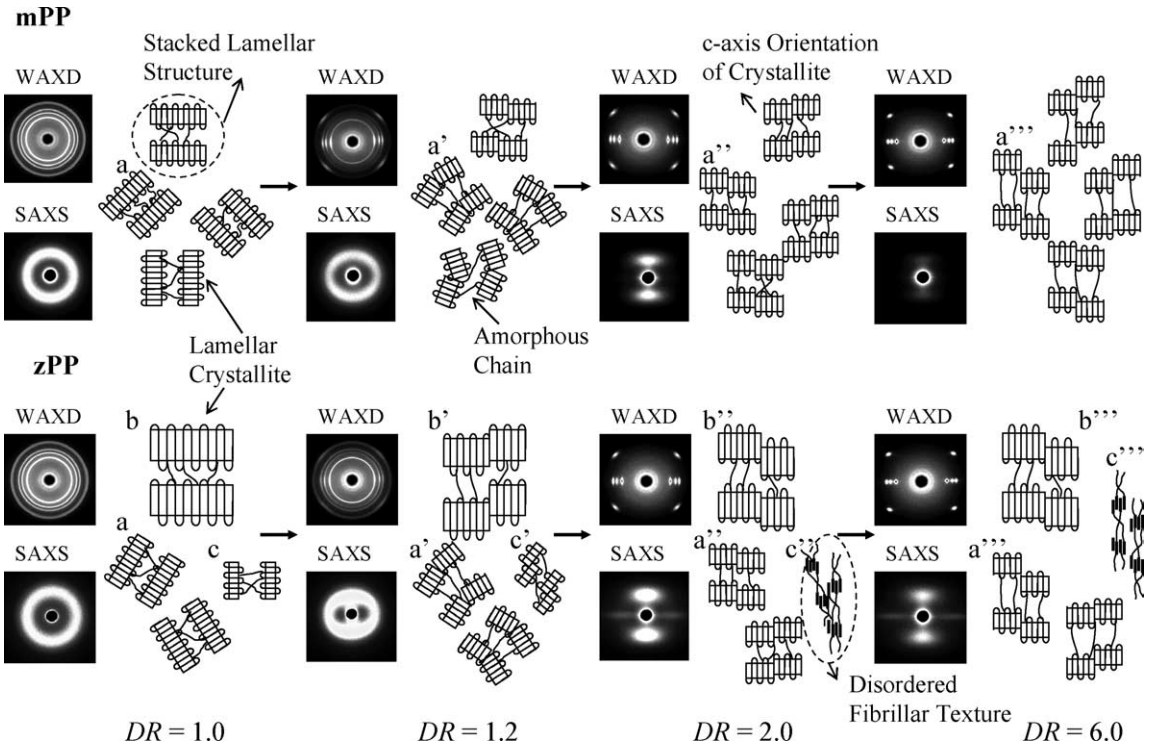

Fig. 15. A schematic illustration of deformation models drawn for mPP and zPP samples, where the meridional direction is the drawing direction. (i) DR = 1.0; unoriented distribution of the regularly stacked lamellar structure. The lamellae of mPP are homogeneous (only the lamellae labeled as a) but those of zPP are heterogeneous (the lamellae with a–c labels). (ii) DR = 1.2; the tilting and sliding of lamellar crystallites occur (a, b, c → a′, b′, c′). (iii) DR = 2.0; the blocks of lamellar structure orient along the drawing direction (a″, b″). The disordered fibrillar structure without any axial register of crystallites (c″) is formed in zPP. (iv) DR = 6.0; the fragmentation of the stacked lamellar structure is developed in mPP (a″ → a‴). In case of zPP, the lamellar structure labeled as a″ is gradually fragmentized (a″ → a‴) and the fibrillar texture labeled c″ is stretched (c″ → c‴). The stacked lamellar structure labeled as b″ is little deformed (b″ → b‴).

internal condition or the characteristic features of iPP sample itself, in particular the slight difference in the MW, MWD and IT distribution. In the present paper we illustrated the structure changes during the hot drawing process on the basis of the already-proposed lamellar models. The deformation of the crystalline polymer sample in the necking region may be interpreted in another type of model, i.e. the melt of stacked lamellae followed by the recrystallization into the oriented fibrillar structure. Further investigation is needed to clarify the deformation behavior in the necking region.

Acknowledgements

The authors would like to thank Mr Ken-ichiro Yada of Sumitomo Chemical Co. Ltd for kindly providing the material. Thanks are also due to Sumitomo Chemical Co. Ltd for permission to publish this paper. This experiment was carried out under the collaborative program between Sumitomo Chemical Co. Ltd and Photon Factory of the ministry of education, culture, sports, science and technology.

References

[1] Brown N, Ward IM. J Mater Sci 1983;18:1405.
[2] Chu JN, Schultz JM. J Mater Sci 1989;24:4538.
[3] Flood JE, Nulf SA. Polym Eng Sci 1990;30:1504.
[4] Fujiyama M, Kitajima Y, Inata H. J Appl Polym Sci 2002;84:2128.
[5] Karacan I, Taraiya AK, Bower DI, Ward IM. Polymer 1993;34:2691.
[6] Alberola N, Fugier M, Petit D, Fillon B. J Mater Sci 1995;30:860.
[7] Stefan R, Ludovic C, Helmut M, Klaus S, Johannes S. Rheol Acta 2002;41:332.
[8] Lin L, Argon AS. J Mater Sci 1994;29:294.
[9] Aboulfaraj M, G'Sell C, Ulrich B, Dahoun A. Polymer 1995;36:731.
[10] Chu F, Yamaoka T, Kimura Y. Polymer 1995;36:2523.
[11] Li JX, Cheung WL, Chan CM. Polymer 1999;40:2089.
[12] Li JX, Cheung WL, Chan CM. Polymer 1999;40:3641.
[13] Liu Y, Truss RW. J Polym Sci, Part B: Polym Phys 1994;32:2037.
[14] Sweeney J, Ward IM. J Rheol 1995;39:861.
[15] Hu WG, Rohr KS. Acta Polym 1999;50:271.
[16] Peterlin A. J Mater Sci 1971;6:490.
[17] Kanig G. J Cryst Growth 1980;48:303.
[18] Hiss R, Hobeika S, Lynn C, Strobl G. Macromolecules 1999;32:4390.
[19] Ran S, Zong X, Fang D, Hsiao BS, Chu B, Ross R. J Appl Cryst 2000; 33:1031.
[20] Ran S, Zong X, Fang D, Hsiao BS, Chu B, Phillips RA. Macromolecules 2001;34:2569.
[21] Somani RH, Hsiao BS, Nogales A, Fruitwala H, Srinivas S, Tsou AH. Macromolecules 2001;34:5902.
[22] Marco Y, Chevalier L, Chaouche M. Polymer 2002;43:6569.
[23] Wiyatno W, Pople JA, Gast AP, Waymouth RM, Fuller GG. Macromolecules 2002;35:8488.

[24] Tashiro K. Rep Prog Polym Phys Jpn 2000;43:219.
[25] Koike Y, Cakmak M. Macromolecules 2004;37:2171.
[26] Spaleck W, Kuber F, Winter A, Rohrmann J, Bachmann B, Antberg M, et al. Organometallics 1994;13:954.
[27] Zambelli A, Locatelli P, Bajo G, Bovey FA. Macromolecules 1975;8:687.
[28] Tsutsui T, Ishimaru N, Mizuno A, Toyota A, Kashiwa N. Polymer 1989;30:1350.
[29] Busico V, Cipullo R, Chadwick JC, Modder JF, Sudmeijer O. Macromolecules 1994;27:7538.
[30] Lin S, Waymouth RM. Macromolecules 1999;32:8283.
[31] Kakugo M, Miyatake T, Naito Y, Mizunuma K. Macromolecules 1988;21:314.
[32] Natta G. J Polym Sci 1955;16:143.
[33] Amemiya Y, Ito K, Yagi N, Asano Y, Wakabayashi K, Ueki T, et al. Rev Sci Instrum 1995;66:2290.
[34] Ito K, Amemiya Y. Jpn J Soc Synchrotron Radiat Res 2000;13:372.
[35] Huang M, Li X, Fang B. J Appl Polym Sci 1995;56:1323.